Fungal Genetics and Biology 45 (2008) 1111–1121

Contents lists available at ScienceDirect

Fungal Genetics and Biology

journal homepage: www.elsevier.com/locate/yfgbi

Quantifying dynamic resource allocation illuminates foraging strategy in *Phanerochaete velutina*

M. Tlalka [1], D.P. Bebber [1], P.R. Darrah, S.C. Watkinson, M.D. Fricker [1,*]

Department of Plant Sciences, University of Oxford, South Parks Road, Oxford OX1 3RB, UK

ARTICLE INFO

Article history:
Received 4 February 2008
Accepted 27 March 2008
Available online 6 April 2008

Keywords:
Phanerochaete velutina
Amino-acid transport
α-Aminoisobutyrate
Fungal foraging behaviour
Photon-counting scintillation imaging
Resource allocation

ABSTRACT

Saprotrophic woodland fungi forage for mineral nutrients and woody resources by extension of a mycelial network across the forest floor. Different species explore at different rates and establish networks with qualitatively differing architecture. However, detailed understanding of fungal foraging behaviour has been hampered by the absence of tools to quantify resource allocation and growth accurately and non-invasively. To solve this problem, we have used photon-counting scintillation imaging (PCSI) to map and quantify nutrient allocation and localised growth simultaneously in heterogeneous resource environments. We show that colonies spontaneously shift to an asymmetric growth pattern, even in the absence of added resources, often with a distinct transition between the two growth phases. However, the extent of polarisation was much more pronounced and focussed in the presence of an additional cellulose resource. In this case, there was highly localised growth, often at the expense of growth elsewhere in the colony, and marked accumulation of ^{14}C-AIB in the sector of the colony with the added resource. The magnitude of the response was greatest when resource was added around the time of the endogenous developmental transition. The focussed response required a metabolisable resource, as only limited changes were seen with glass fibre discs used to mimic the osmotic and thigmotropic stimuli upon resource addition. Overall the behaviour is consistent with an adaptive foraging strategy, both to exploit new resources and also to redirect subsequent foraging effort to this region, presumably with an expectation that the probability of finding additional resources is increased.

1. Introduction

Saprotrophic, cord-forming fungi form extensive networks at the soil-litter interface as they search for new resources in the patchy woodland environment. Different species exhibit qualitatively different foraging strategies, ranging from slow, but intensive exploration by a diffuse colony margin of fine hyphae, to more open systems with rapidly growing cords that are thought to be better suited to discovery of large, sparsely distributed resources (Boddy, 1999; Boddy and Jones, 2007; Tlalka et al., 2008). Persistent networks may also operate a 'sit and wait' strategy, ready to capitalise rapidly on ephemeral input of new resources (Boddy, 1999; Boddy and Jones, 2007). Within this broad overall framework, the precise pattern of growth and development for any individual colony is sensitive to the resource status of the initial inoculum, the quality and quantity of resources encountered, the order they are discovered, the degree of competition from other fungi, and a range of microclimatic and edaphic factors (Boddy, 1999; Boddy and Jones, 2007). Changes in foraging behaviour appear to involve integrated responses across the whole colony that result in co-ordinated decisions on resource allocation and growth even between remote regions. For example, local encounter with a substantial new resource triggers strengthening of cords to the new resource, cessation of growth elsewhere, followed by initiation of a new growth front from the resource and regression of more distal parts of the mycelium (Boddy and Jones, 2007; Fricker et al., 2008; Tlalka et al., 2008).

Changes in colony organisation are also accompanied by shifts in nutrient uptake, storage and translocation patterns that are thought to be needed to exploit the new resource, recycle redundant mycelium and drive new exploration (Lindahl et al., 2004; Boddy and Jones, 2007; Fricker et al., 2008; Tlalka et al., 2008). However, experimentally measured allocation of $^{32}PO_4$ gives a more complex picture of changing source–sink relationships as new resources are added (Boddy and Jones, 2007; Fricker et al., 2008), suggesting our knowledge of actual source and sink relationships, and how they change over time, is relatively primitive (Lindahl et al., 2004). For example, whilst there is preferential allocation to larger resources, particularly during the early phase of colonisation, resources also accumulate in existing resource bases that could act as reserves for valuable nutrients (Watkinson et al., 2006; Boddy and Jones, 2007; Tlalka et al., 2008). To under-

* Corresponding author. Fax: +44 (0) 1865 275074.
E-mail address: mark.fricker@plants.ox.ac.uk (M.D. Fricker).
[1] These authors contributed equally to this paper.

1087-1845/$ - see front matter © 2008 Elsevier Inc. All rights reserved.
doi:10.1016/j.fgb.2008.03.015

stand the underlying signalling events and molecular changes associated with foraging behaviour demands visualisation techniques and analysis tools that can identify the location and timing of both morphological and physiological responses.

Morphological changes in foraging behaviour can be detected as changes in radial extension rate, area covered or fractal dimension (Bolton and Boddy, 1993; Boddy et al., 1999; Boddy and Donnelly, 2008). Fractal dimension in particular provides a measure of space-filling that gives good discrimination between diffuse foraging by fine hyphae in comparison to more open corded networks. Nevertheless, as fractal dimension is a global property of the whole colony, it tends to disguise the origin of local spatial structure that actually leads to polarisation of the colony in response to encounter with a new resource, although it is possible to calculate fractal dimensions from sub-regions of the image (Boddy and Donnelly, 2008). Image analysis of the sectors with and without resource has provided some basic spatial resolution and is able to detect responses at earlier time points than unaided visual observation (Wells et al., 1998b; Harris and Boddy, 2005). However, there is still a substantial lag before sufficient morphological change is apparent by these methods. It is likely that the system responds much more quickly than these data would indicate, and suggests that more refined analytical tools are necessary to detect early alterations in colony architecture.

With the development of photon-counting scintillation imaging (PCSI, Tlalka et al., 2002, 2003, 2007; Fricker et al., 2007), it has been possible to map the distribution of the non-metabolised, amino-acid analogue, α-aminoisobutyrate (^{14}C-AIB) during the development of small mycelial networks of *Phanerochaete velutina* in spatially heterogenous resource environments. We have previously shown that ^{14}C-AIB was taken up rapidly and distributed throughout the colonies, with a marked pulsatile component to transport that was organised into well demarcated domains that differed in the phase of the oscillations (Tlalka et al., 2003, 2007; Fricker et al., 2007). During these studies, a transition from symmetrical to asymmetric growth and differential N-resource allocation was observed, both in control colonies and to a greater extent following addition of an additional cellulose resource (Tlalka et al., 2007). These responses are analogous to those reported on the larger scale soil/wood microcosm systems (Dowson et al., 1988a, 1988b, 1988c; Bolton and Boddy, 1993; Donnelly et al., 1995; Wells et al., 1997, 1998a; Donnelly and Boddy, 1998; Boddy et al., 1999; Boddy and Donnelly, 2008), and suggest that such microcosms may provide a tractable experimental system to quantify both foraging behaviour and resource allocation with good temporal and spatial resolution.

In this paper, we develop new analysis tools to quantify: first, the extent of symmetry breaking in control colonies, that occurs as part of a normal developmental progression in foraging behaviour; second, the magnitude of colony polarisation in response to both thigmotropic and nutritional cues, including developmental control of the sensitivity as the colony increases in size; and third, the relationship between localised extension rate and preferential N-allocation. Overall the behaviour is consistent with an adaptive foraging strategy both to exploit new resources and also to redirect subsequent foraging effort to this region, presumably with an expectation that the probability of finding additional resources is increased.

2. Materials and methods

2.1. Fungal material

Cultures of *Phanerochaete velutina*, from the Cardiff culture collection were grown on 2% malt agar (2% Oxoid malt extract, 2% Oxoid No.3 agar) at 22 ± 1 °C in darkness as previously described (Tlalka et al., 2002, 2003).

2.2. Experimental microcosms

Small artificial microcosms were prepared as in Tlalka et al. (2002, 2003). Briefly, a circular 12 mm sub-marginal inoculum of *P. velutina* was placed mycelial surface down in a 120 mm square Petri dish on top of either a Lite Plus intensifying screen (Sigma, Poole, UK) or a BioMax TranScreen LE intensifying screen (Sigma, Poole, UK). In experiments examining resource addition, an additional 13 mm cellulosic resource (Grade AA filter paper disc, Whatman, Maidstone, England) or a 13-mm glass fibre disc, punched from a 24-mm GF/C disc (Whatman, Maidstone, England), was added 20–30 mm away from the inoculum once the colony had grown 30–40 mm, typically after 90–144 h. Responses were then followed for a further 144 h or until the colony reached the edge of the microcosm. Humidity was maintained by the presence of water in small (500 μl) containers and by sealing the sample dishes with Parafilm (American National Can™, Neenah, NI, USA) or by placing microcosms in a sealed Perspex chamber with dishes containing water saturated sand.

2.3. Visualisation of ^{14}C-AIB transport using photon-counting scintillation imaging

^{14}C-AIB was imaged using a high-resolution, photon-counting camera system (HRPCS-3, Photek Inc., St Leonards on Sea, UK) equipped with a Nikon 28 mm f/2 or Nikon 50 mm f/1.2 lens as described previously (Tlalka et al., 2003, 2007). The (*x*,*y*) pixel dimensions ranged between 0.39 and 0.46 mm, depending on the number and arrangement of the microcosms, with up to six microcosms imaged in parallel. About 20–25 μl (46.3 kBq) of a 0.9 mM solution of 2-amino[1-^{14}C]isobutyric acid, ^{14}C-AIB (Amersham, UK) in distilled water (specific activity 2.11 GBq mmol^{-1}) was applied to the centre of the inoculum. The chambers were then sealed and placed in continuous darkness in the camera imaging box at 21 ± 0.5 °C. The temperature was continuously monitored with "Diligence"™ data loggers (Comark Ltd., UK). Images were integrated over 60 min. periods and exported as 8-bit uncompressed *avi*-format files from the Photek environment.

2.4. Sector-based analysis of radial extension and ^{14}C-AIB distribution

Time-series *avi* movies were analysed in the MatLab environment using a custom software interface (available on request from MDF). The inoculum and resource were manually delineated and a correction factor applied to compensate for the attenuation of the light signal passing through the different media (3× for filter paper, 2× for glass fibre and 1.5–3× for the inoculum depending on thickness). Estimates of the radial extension rate were made following grey-level segmentation of the ^{14}C-AIB scintillation image. Contrast limited adaptive histogram (CLAHE, Pizer et al., 1987) was used to bring the edges of the mycelium up to similar contrast levels, even though the absolute original intensity varied by almost an order of magnitude, whilst suppressing the background noise. A segmentation threshold was determined automatically using Otsu's method (Otsu, 1979), that finds the value that minimises the between class variance of a bi-modal distribution comprising background and object. The resultant binary image was median filtered and any internal holes that emerged after the local contrast stretching were automatically filled. To validate this approach, colonies were grown across 1.4 μm Mylar film (Isotope imaging film 1.4 μm FlushTec, Cathedral City, CA), labelled with ^{14}C-AIB and imaged for 197 h. The colony was then lifted from the screen and imaged against a black background at

2560 × 1920 (Sony DSC-F717 digital still camera equipped with a +2 converter) to give a nominal pixel size of 5 × 5 μm. The AIB distribution map and the perimeter of the automatically segmented area were superimposed on the red and green channels of the bright-field image (Supplementary Fig. 1). There was very good correspondence between the automatically segmented area and the visible distribution pattern of the colony, with only the very finest leading hyphae clipped as a result of the low signal and median filtering.

As the radial extension was not symmetrical, extension rates were determined for eight equal sectors radiating out from the inoculum, with the mid-line of the first sector aligned to the inoculum–resource axis. In un-treated systems the axis was aligned to the horizontal image *x*-axis. The average radius of the colony was determined for each sector and the extension rate determined from a 12 or 24 h rolling average.

The distribution of ^{14}C-AIB in each sector was calculated as the sum of the total pixel intensity and expressed as a percentage distribution in each sector to accommodate varying absolute levels of uptake and distribution in each experiment.

2.5. Analysis of radial extension and ^{14}C-AIB distribution using circular statistical measures

Whilst changes in the coefficient of variation between the different sectors provided a crude measure of symmetry breaking, angular measures of radial extension and resource allocation were developed to provide a more detailed quantitative analysis of colony responses. Thus, the asymmetry in radial extension was assessed from the displacement of the centre of growth, averaged over a 12 h window, from the centre of the inoculum and expressed as a vector with magnitude ($\overline{R}_{RE}$) and direction ($\overline{\theta}_{RE}$). The co-ordinates of the centre of growth were calculated from the centroid of the segmented area:

$$\overline{X} = \frac{1}{n}\sum_{i=1}^{n} x_i, \quad \overline{Y} = \frac{1}{n}\sum_{i=1}^{n} y_i \tag{1}$$

where n was the total number of pixels in the segmented area. The magnitude of the resultant vector from the inoculum was given by:

$$\overline{R}_{\mathrm{RE}} = \sqrt{\overline{X}^2 + \overline{Y}^2}, \tag{2}$$

The alignment of the vector with the added resource, when present, was given by:

$$\overline{\theta}_{\mathrm{RE}} = \arctan 2\left(\frac{y_r}{x_r}\right) - \arctan 2\left(\frac{\overline{Y}}{\overline{X}}\right) \tag{3}$$

where x_r and y_r were the (x,y) co-ordinates of the added resource. In control colonies, $\bar{\theta}_{\mathrm{RE}}$ was measured with respect to the *x*-axis.

To give an estimate of how tightly the growth was focussed in a particular direction, the angular mean vector ($\bar{r}_{\mathrm{RE}}$) was calculated from the individual angles ($a_1 \ldots a_n$) of each pixel in the area images as follows:

$$\bar{r}_{\mathrm{RE}} = \sqrt{\left(\frac{\sum_{i=1}^{n}\cos a_i}{n}\right)^2 + \left(\frac{\sum_{i=1}^{n}\sin a_i}{n}\right)^2} \tag{4}$$

$\bar{r}_{\mathrm{RE}}$ was then used to estimate the circular standard deviation:

$$s_{0,RE} = \frac{180}{\pi}\sqrt{-2\ln \bar{r}_{\mathrm{RE}}} \tag{5}$$

A similar sequence of operations was used to characterise allocation of ^{14}C-AIB, except values were weighted by the intensity (I_i) of the ^{14}C-AIB signal at each pixel. Thus the magnitude and direction of the displacement for the centre of mass for ^{14}C-AIB were calculated as:

$$\overline{R}_{\mathrm{AIB}} = \sqrt{\left(\frac{\sum_{i=1}^{n} I_i x_i}{\sum_{i=1}^{n} I_i}\right)^2 + \left(\frac{\sum_{i=1}^{n} I_i y_i}{\sum_{i=1}^{n} I_i}\right)^2} \tag{6}$$

$$\overline{\theta}_{AIB} = \arctan 2\left(\frac{y_r}{x_r}\right) - \arctan 2\left(\frac{\sum_{i=1}^{n} I_i y_i}{\sum_{i=1}^{n} I_i x_i}\right) \tag{7}$$

The circular standard deviation was calculated from the angular mean of the individual angles ($a_1 \ldots a_n$) to each pixel, weighted by their intensity value ($I_1 \ldots I_n$):

$$\bar{r}_{AIB} = \sqrt{\left(\frac{\sum_{i=1}^{n} I_i \cos a_i}{\sum_{i=1}^{n} I_i}\right)^2 + \left(\frac{\sum_{i=1}^{n} I_i \sin a_i}{\sum_{i=1}^{n} I_i}\right)^2} \tag{8}$$

$\bar{r}_{AIB}$ was then used to calculate the circular standard deviation of the mean angle describing the direction of ^{14}C-AIB allocation:

$$s_{0,\mathrm{AIB}} = \frac{180}{\pi}\sqrt{-2\ln \bar{r}_{\mathrm{AIB}}} \tag{9}$$

Symmetrical colonies would be predicted to have displacements close to zero and large circular standard deviations, whilst highly polarised colonies would show much larger displacements and small circular deviations. The overall behaviour of individual colonies was visualised by plotting the centre of growth on the contour plot, and the centre of mass of ^{14}C-AIB on the ^{14}C-AIB scintillation image.

The mean of the alignment angle from different experiments and the statistical significance of the angular distributions were calculated using Oriana 2.00 (Kovach Computing Services, Anglesey, Wales).

2.6. Statistical modelling of responses

Changes in $\overline{R}_{\mathrm{RE}}$ and $\overline{R}_{\mathrm{AIB}}$ were fit with Linear Mixed Effects (LME) models using maximum likelihood methods. In the case of repeated measures data, random effects refer to the subjects that have been measured repeatedly through time, while fixed effects refer to treatments applied to those subjects. LME models are more robust than repeated measures ANOVA models when the assumption of 'circularity' or 'sphericity' (equal within-subjects variances) is not met. In the fitted model, the response variable was $\overline{R}$, the fixed effect was treatment, the random effect was colony replicate and the time was treated as a covariate to be modelled with a polynomial curve. $\overline{R}_{\mathrm{AIB}}$ data were square root-transformed prior to analysis, to remove observed heteroskedasticity. Polynomial coefficients to 3rd order were fitted for each treatment, and random intercepts for each replicate. In practice, 2nd order fits gave no improvement over linear regression for $\sqrt{\overline{R}_{\mathrm{AIB}}}$ and only a very marginal improvement for $\overline{R}_{\mathrm{RE}}$, thus linear fits were used for both. Temporal autocorrelation among data was modelled using a serial autoregressive function. Analysis was conducted using the *lme* procedure of the *nlme* package version 3.1–48 (Pinheiro and Bates, 2000) for R 1.9.0 (R Development Core Team, 2007).

3. Results

3.1. Radial extension and ^{14}C-AIB distribution in nutrient limited colonies

In all experiments (n = 42), extension over the first 72–96 h prior to resource addition occurred as fine, un-corded mycelium radiating symmetrically from the inoculum (Fig. 1, first column). Even in the absence of added resources, symmetrical extension slowed or even stopped temporarily at around 96–144 h, to be replaced by sparser and more polarised extension over a broad sector of the colony (Fig. 1A) or, more often, from a number of more limited segments of the margin (Fig. 1B; see also Supplementary Movie 1). The asymmetry in extension pattern was visualised in

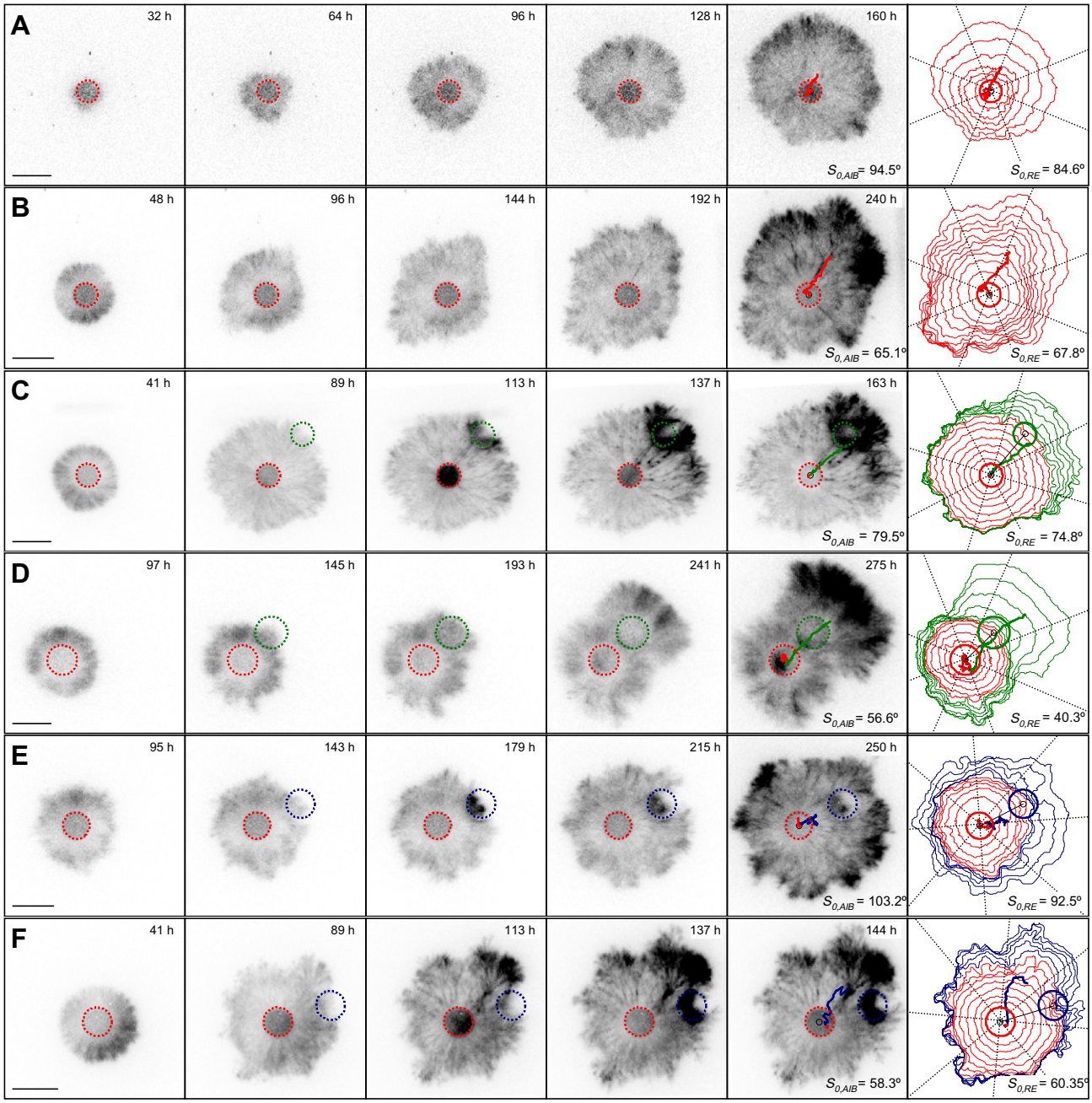

Fig. 1. Polarised extension and resource allocation in foraging colonies of *Phanerochaete velutina*. The uptake and distribution of ^{14}C-AIB was followed continuously using photon-counting scintillation imaging (PCSI) in colonies of *Phanerochaete velutina* growing from an agar inoculum (marked with a dotted red circle) across an inert scintillation screen with no additional resources (A,B), in the presence of filter paper resources (green circle, C,D), or glass fibre resources (blue circle, E,F). Each image represents a 1 h integration of the photon counts from the scintillation screen at the time point given and two examples are shown for each treatment to illustrate the range of responses observed. The final image in the series shows a contour plot of the segmented area of the colony at 12 h (C,F) or 24 h intervals (A,B,D,E), with the colour transition indicating the time of new resource addition. The radiating sectors for the extension rate analysis and their alignment to the position of the resource (when present) are also shown. A track of the centre of mass of the ^{14}C-AIB distribution is superimposed on the final scintillation image, and the corresponding track for the centre of radial extension superimposed on the extension contour plot, with the colour transition indicating the addition of the new resource. The angular spread of ^{14}C-AIB or radial extension is given by the circular standard deviation ($s_{0,AIB}$ and $s_{0,RE}$, respectively). Scale bar = 25 mm.

contour plots of the segmented boundary (Fig. 1, last column), and quantified as the average extension in each of eight sectors spaced at 45° around the colony (e.g. Fig. 2A). Extension in all sectors was comparable initially, but became divergent following the transition to the second phase of sparser asymmetrical extension, even in colonies with no additional resources (Fig. 2A).

The radial extension rate for each sector in untreated colonies, calculated as the gradient of the extension data over time, showed an early peak at 30–60 h, followed by a general reduction before the transition to the second phase (e.g. Fig. 2B). The second phase itself was characterised by a marked increase in variance of the sector extension rates (Fig. 2B), with the most rapidly growing sectors (marked with an asterisk in Fig. 2A) reaching similar rates to the first extension phase. However, extension in the other sectors was reduced 4- to 5-fold, giving an increase in the coefficient of variation (cv) between sectors (Fig. 2C). Similar observations were made in 13 other control systems. The average extension rate for all 14 control systems was 140 ± 50 μm h^{-1} before the transition, and 130 ± 20 μm h^{-1} in the second phase (Table 1). The coefficient of variation (cv) between all eight sectors across replicates was

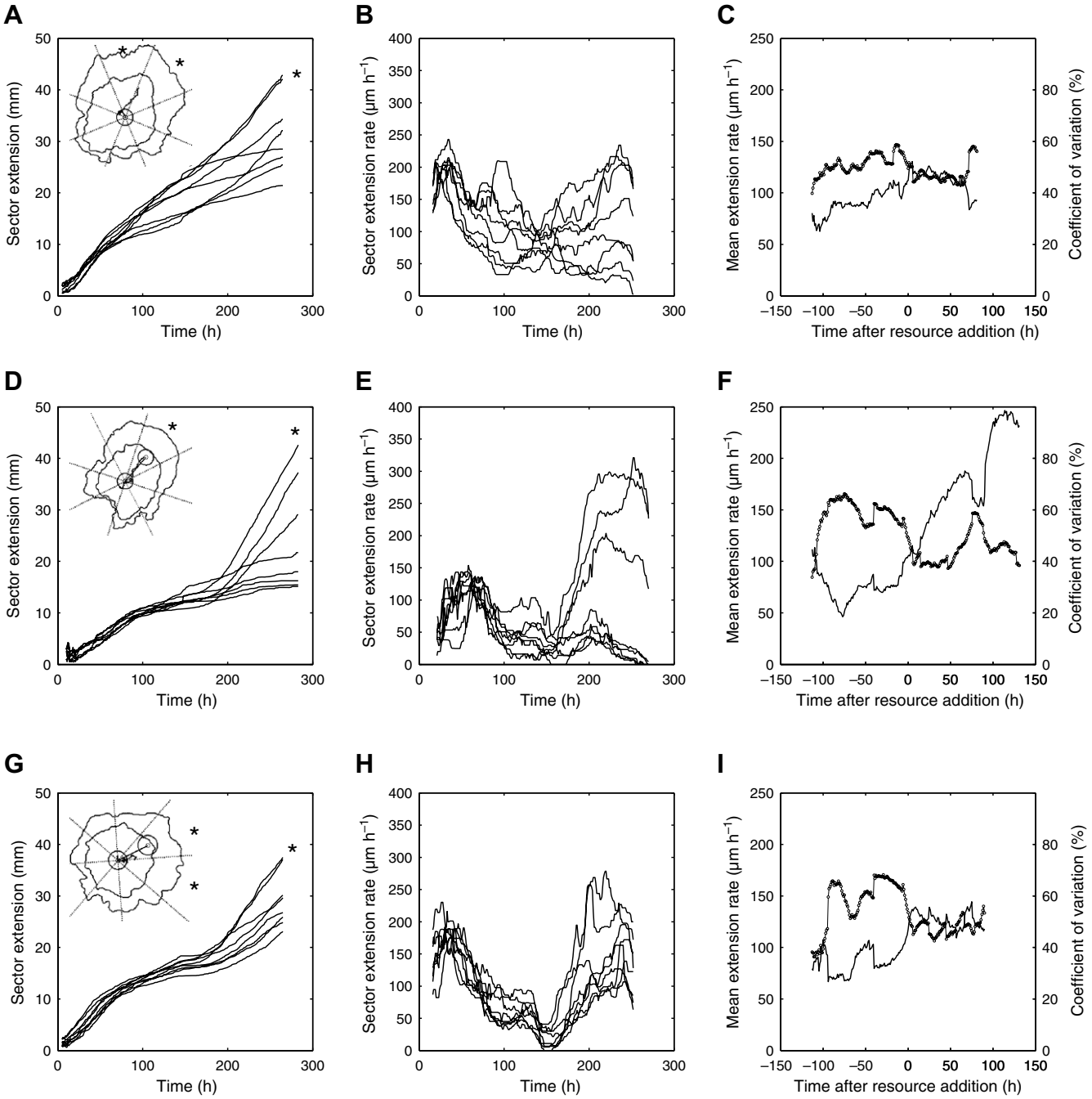

Fig. 2. Sector-based analysis of polarised extension. The average increase in extension for each 45° sector is shown for an untreated colony (A), or colonies supplemented with filter paper (D) and glass fibre (G) resources. These colonies correspond to the colonies shown in B, D and E, respectively from Fig. 1. The extension rate for each sector was calculated as the gradient of the average sector extension (B, E and H). The extension rate between sectors was similar initially, increasing to a maximum at 30–50 h before declining prior to the transition to asymmetric extension around 100 h. Following the transition, there was considerably greater variance in the rate of extension between the different sectors, even in the untreated colonies (B). The greatest variation was in colonies with added filter paper (E). The mean rate of extension (dotted lines) across all sectors and replicates (C, F and I) averaged ~150 μm h^{-1} during the symmetric extension phase and then dropped to ~120 μm h^{-1} following the transition to asymmetric extension. In contrast, the coefficient of variation (solid line), showed a small increase from ~40% in the untreated (C, $n = 14$) and glass fibre (I, $n = 13$) experiments, but a substantial change increasing to ~100% in the filter paper treated colony (F, $n = 15$).

40.7 ± 5.0% during initial extension, and increased slightly by 1.23-fold with the transition to more asymmetric growth (Table 1).

In general, the distribution of ^{14}C-AIB matched the extension pattern, as higher levels of AIB were associated with regions of more rapid extension (e.g. Fig. 1A and B). The transition between the two extension phases was often accompanied by a substantial increase in the uptake of AIB and the appearance of cords in the radiolabel images (e.g. Fig. 1B). In the initial, more symmetrical extension phase, the maximum ^{14}C-AIB distribution in any sector was 22.7 ± 1.6%, and increased slightly by 1.13-fold following the transition to sparser extension (Table 1). This compares to a prediction of 12.5% in each sector if allocation was uniform.

3.2. The effect of added resources on radial extension and ^{14}C-AIB allocation

In colonies supplemented with a filter paper disc, the extent of polarised extension was much more pronounced, and was highly

Table 1
Summary of sector-based measurements and angular measures of radial extension and ^{14}C-AIB distribution in developing colonies of *Phanerochaete velutina*

		Control (n = 14)		Cellulose resource (n = 15)		Glass fibre disc (n = 13)	
		Before[a]	After[b]	Before[a]	After[b]	Before[a]	After[b]
Sector based measurements							
Average sector radial extension (μm h^{-1})[c]		140 ± 50	130 ± 20	156 ± 36	110 ± 17	151 ± 32	119 ± 26
Coefficient of variation of sector radial extension (%)[c]		40.7 ± 5.0	50.0 ± 6.2	37.4 ± 5.5	69.7 ± 8.8	45.8 ± 7.1	50.1 ± 9.3
Max amount of ^{14}C-AIB per sector (%)[c]		22.7 ± 1.6	25.7 ± 1.6	20.0 ± 1.3	41.1 ± 3.8	23.9 ± 2.2	25.0 ± 2.0
Angular measures of radial extension							
Displacement of the centre of radial extension (mm)[c]	$\bar{R}_{RE}$,	6.7 ± 0.7	14.8 ± 1.9	7.4 ± 1.4	24.8 ± 2.3	10.1 ± 1.5	11.5 ± 1.5
Alignment of $\bar{R}_{RE}$ to resource axis (°)[d]	$\bar{\theta}_{RE}$		144 ± 59.6		−16.3 ± 41.7		−11.3 ± 94.8
Circular standard deviation of radial extension (°)[c]	$s_{o,RE}$		82.9 ± 4.2		55.5 ± 6.1		87.0 ± 5.1
Angular measures of ^{14}C-AIB allocation							
Displacement of ^{14}C-AIB centre of mass (mm)[c]	$\bar{R}_{AIB}$	3.7 ± 0.4	8.7 ± 2.5	4.3 ± 1.3	22.3 ± 1.5	6.6 ± 1.3	8.3 ± 1.2
Alignment of $\bar{R}_{AIB}$ to resource axis (°)[d]	$\bar{\theta}_{AIB}$		144 ± 62.0		−14.9 ± 28.0		−1.3 ± 91.0
Circular standard deviation of ^{14}C-AIB (°)[c]	$s_{o,AIB}$		109 ± 10.7		57.7 ± 4.2		102 ± 13.7

[a] Before, represents the value averaged over 108 h before the time of resource addition (or the equivalent time in control experiments) for sector based measurements, or averaged over 24 h before the time of resource addition for angular measures.
[b] After, represents the value averaged over 108 h after the time of resource addition (or the equivalent time in control experiments) for sector based measurements, or averaged between 84 and 108 h for angular measures.
[c] Values are given as the means ± SEM.
[d] Values are given as angular means ± circular standard deviation.

localised to the sector of the colony containing the new resource (Fig. 1C and D; see also Supplementary Movie 2). Extension was initially even amongst all sectors (e.g. Fig. 2D), as with the un-treated colonies. Following resource addition and the transition to the second phase, the extension rate increased dramatically in the sector with the new resource, with extension dropping to zero on the opposite side of the colony (Fig. 2E). Results averaged across all eight sectors and fifteen replicates showed a slight decline in average radial sector extension rate following addition of the new resource from 156 ± 36 μm h^{-1} to 110 ± 17 μm h^{-1} (Fig. 2F). The coefficient of variation between sectors showed a substantial increase following resource addition, reflecting the pronounced asymmetry in extension amongst the different sectors. The value for all replicates averaged for 108 h prior to resource addition was 37.4 ± 5.5%, whilst the value averaged for 108 h after resource addition was 69.7 ± 8.8% (Table 1). In practice, the difference in extension rate between the sectors continued to increase following resource addition and the cv reached 100 ± 13% by 108 h (Fig. 2F). In parallel with the changes in extension following addition of the new resource, a high percentage (41.1 ± 3.8%) of the total ^{14}C-AIB was present in the sector of the colony containing the resource (Table 1, Fig. 1C and D). Strongly labelled cords were apparent between the inoculum and resource. In some replicates (e.g. Fig. 1C; see also Supplementary Movie 2), label was concentrated in the new resource itself, although detection of signal in this region was complicated by absorption of the β-particles from ^{14}C-AIB and attenuation of light emission by the resource itself. As extension in the sector with the new resource continued, high levels of ^{14}C-AIB accumulated in the peripheral growth zone extending beyond the resource (Fig. 1C and D).

The colony response to a moist glass fibre disc was tested to determine whether the responses observed with the filter paper resource were specifically linked to sensing of a new food resource or resulted from physical stimulation or increased water availability upon resource addition. A local increase in ^{14}C-AIB was observed in the glass fibre disc (Fig. 1E and F; see also Supplementary Movie 3). However, ^{14}C-AIB continued to be distributed to other sites on the colony margin (Fig. 1E), particularly if these were already developing as a new growth zone (Fig. 1F). Likewise, the sector extension was asymmetrical, with local stimulation of extension rate (Fig. 2G and H), but the overall response was closer to the control than the filter paper resources and did not show good alignment with the location of the resource (Fig. 1E and F). The average extension rate for all replicates decreased slightly from 151 ± 32 μm h^{-1} during the first phase to 119 ± 26 μm h^{-1} following resource addition (Table 1, Fig. 2I). There was a small (1.1-fold) increase in the coefficient of variation for extension amongst sectors, reflecting the slight asymmetry in extension (Table 1 and Fig. 2I). The distribution of ^{14}C-AIB was similar to control systems, with 25.0 ± 2.0% present in the faster growing sector (Table 1, Fig. 1E and F).

3.3. Quantitation of directional growth and N-allocation

Whilst changes in the coefficient of variation between the different sectors provided a crude measure of symmetry breaking, angular measures of resource allocation and extension rate provided a more detailed quantitative analysis of colony responses. The centre of radial extension was located at the centre of the inoculum during symmetrical growth, but shifted progressively away with the onset of asymmetrical growth (Fig. 1, last column). Likewise the centre of mass of ^{14}C-AIB was displaced towards the site of preferential growth as the colony became more polarised (Fig. 1, penultimate column; see also Supplementary Movie 1). Whilst all colonies showed an increase in the magnitude of the vector from the inoculum to the centre of radial extension ($\bar{R}_{RE}$, Fig. 3A–C) or the centre of mass of ^{14}C-AIB ($\bar{R}_{AIB}$, Fig. 3G–I) with the transition to asymmetric growth, the effect was more pronounced in colonies with additional cellulose resources (Fig. 3B and H). Between 84 and 108 h after resource addition, $\bar{R}_{RE}$ was 1.7- and 2.2-fold higher for colonies with added cellulose resources in comparison with colonies with no added resources or glass fibre discs, respectively (Table 1). The magnitude of the response to cellulose resources was even greater for $\bar{R}_{AIB}$, with corresponding values of 2.6- and 2.7-fold, respectively (Table 1).

The extent that radial extension and ^{14}C-AIB distribution were focussed in one direction was assessed from the circular standard deviation, $s_{0,RE}$ and $s_{0,AIB}$ (Fig. 1 and Table 1). In general, $s_{0,RE}$ was very broad for both un-treated and colonies with glass fibre dics, but showed a much tighter distribution for colonies with cellulose resources (Table 1). The spread in the distribution of $s_{0,AIB}$ was marginally higher than $s_{0,RE}$, but followed the same trend, with a much tighter distribution in colonies with cellulose resources.

The response to the filter paper was not only greater in magnitude and tightly grouped, but also closely aligned towards the resource (Fig. 3E and K) with a deviation of only a few degrees for

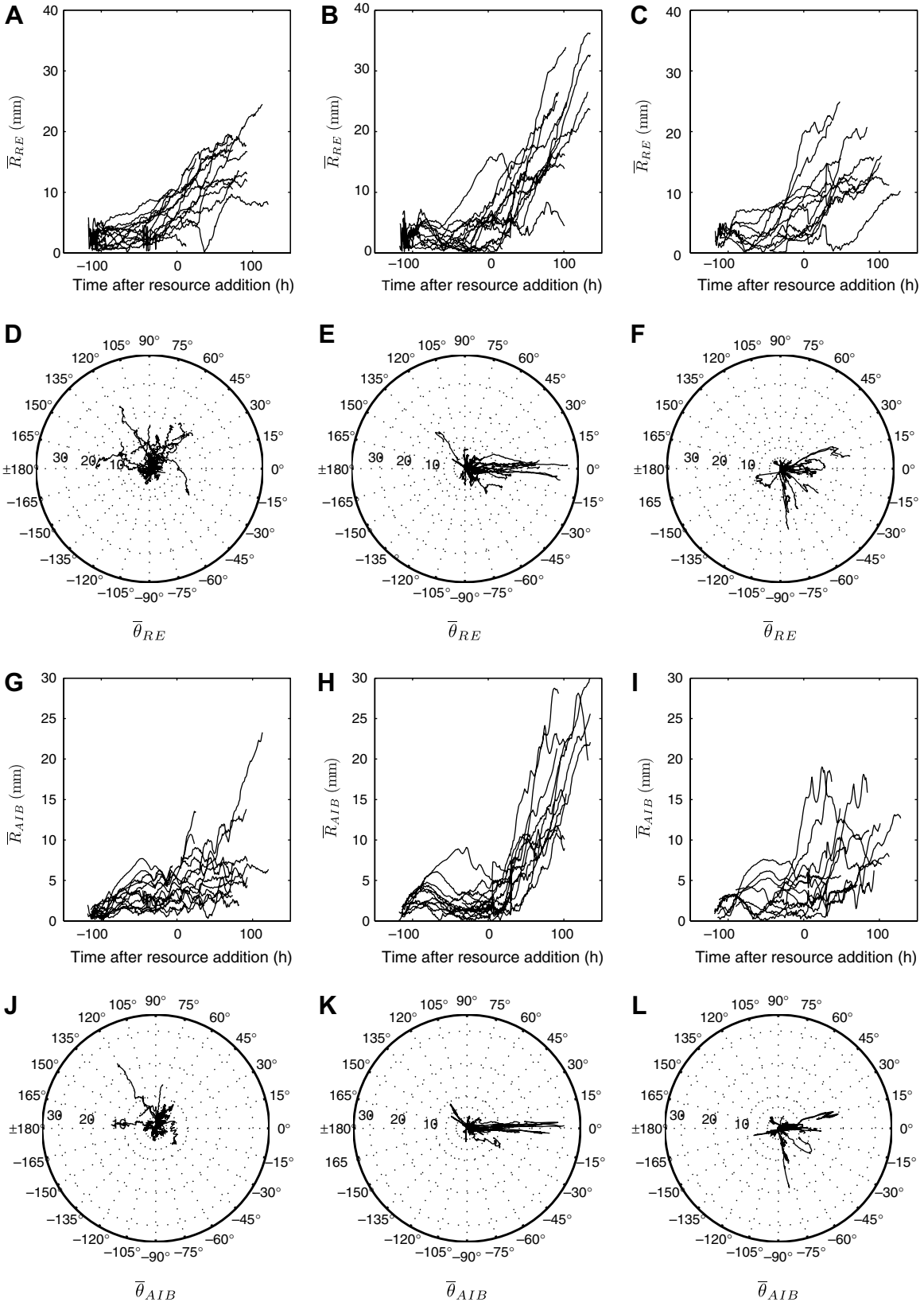

Fig. 3. Magnitude and alignment of the extension vector and allocation of AIB. The magnitude (A–C) and alignment (D–F) for the vector describing the displacement of the centre of extension for all replicate experiments for untreated (A,D), filter paper (B,E) and glass fibre (C,F) are shown normalised to the time after resource addition (or the equivalent time point in untreated colonies). The transition to asymmetric extension is reflected by the increase in the shift of the centre of extension away from the centre of the inoculum (A–C). However, in the case of the filter paper treatment, the magnitude was much greater (B) and the response was tightly aligned to the direction of the resource, with a deviation of only a few degrees from the inoculum-resource vector, set at 0° (E). In the case of the untreated (D) and glass fibre treated (F), the response was more random in direction. Likewise the shift in the centre of mass for ^{14}C-AIB was much more marked and tightly aligned in the filter paper treated colonies (H,K) in comparison to the untreated (G,J) and glass fibre treated (I,L) colonies.

both radial extension and ^{14}C-AIB distribution ($\overline{\theta}_{RE} = -16.3 \pm 41.7^{\circ}$, $p < 10^{-4}$ and $\overline{\theta}_{AIB} = -14.9 \pm 28^{\circ}$, $p < 10^{-6}$) for the time-averaged angle from the vector between the inoculum and resource (Table 1). There was no statistically significant alignment in the control systems as expected (Fig. 3D and J and Table 1). The average responses to glass fibre discs appeared to show some alignment to the resource (Fig. 3F and L), but were not well grouped between experiments, with large circular standard deviations ($\overline{\theta}_{RE} = -11.3 \pm 94.8^{\circ}$ and $\overline{\theta}_{AIB} = -1.3 \pm 91.0^{\circ}$, Table 1) that were not significantly different from an even distribution ($p > 0.44$ and $p > 0.35$, respectively).

3.4. Temporal evolution of responses

The average values reported in Table 1 are taken at particular time intervals with respect to the time of resource addition. However, inspection of the individual colony responses (Fig. 3A–C and Fig. 3G–I) showed that the was some variation in the delay before initiation of the shift in $\overline{R}_{RE}$ and $\overline{R}_{AIB}$, but considerable similarity in the rate of displacement once initiated. The average value for the change in centre of extension ($\Delta\overline{R}_{RE}$) or AIB ($\Delta\overline{R}_{AIB}$) over time for controls was 86 ± 17 μm h^{-1} and 63 ± 16 μm h^{-1}, respectively (Table 2). Average values for the glass fibre treatments were not significantly different at 92 ± 22 μm h^{-1} ($p > 0.3$) and 73 ± 22 μm h^{-1} ($p = 0.39$), respectively. However, the average gradient with filter paper resources was 2.1-fold greater for $\Delta\overline{R}_{RE}$ ($p < 0.0001$) and 2.7-fold greater for $\Delta\overline{R}_{AIB}$ ($p < 0.0001$, Table 1). The models explained 45% and 48% of variation in $\overline{R}_{RE}$ and $\sqrt{\overline{R}_{AIB}}$, respectively.

3.5. Correlation of growth and N-allocation with developmental stage

Although both extension and AIB allocation responded to addition of a cellulose resource, the magnitude of the response appeared to be strongest when the resource was added to colonies before or shortly after the transition from symmetric to asymmetric extension. As the timing of the transition in individual colony development was highly variable, the developmental stage was defined using bi-logistic curves fit to the overall extension data to identify the different growth phases more precisely for each colony (e.g. Fig. 4A). In 24 cases, two phases could be clearly identified using this approach. For these experiments, parameters for the first phase were regarded as the most reliable, as only the start of the second phase was captured in the experiments. The data were therefore normalised to the time when 90% of the first phase was complete, which also corresponded visually to the start of the second phase (Fig. 4A). Values of $\Delta\overline{R}_{RE}$ and $\Delta\overline{R}_{AIB}$ showed a negative dependence on the time of the predicted transition from symmetrical to asymmetric extension (Fig. 4B and C, respectively). On this basis, the sensitivity of the system to resource addition for both $\Delta\overline{R}_{RE}$ and $\Delta\overline{R}_{AIB}$ declined with increasing time after the transition to asymmetric extension, with the regression accounting for a reasonable proportion of the variance in the data ($R^2 = 55\%$ for $\Delta\overline{R}_{RE}$ and $R^2 = 24\%$ for $\Delta\overline{R}_{AIB}$).

Table 2
Changes in extension and ^{14}C-AIB allocation in response to new resources

	$\Delta\overline{R}_{RE}$ (μm h^{-1})	Normalised response	$\Delta\overline{R}_{AIB}$ (μm h^{-1})	Normalised response	n
Control	86 ± 17	1	63 ± 16	1	14
Filter paper	177 ± 21	2.06	169 ± 20	2.68	15
Glass fibre	92 ± 22	1.07	73 ± 22	1.16	13

The displacement in the centre of radial extension ($\overline{R}_{RE}$) or centre of mass for ^{14}C-AIB ($\overline{R}_{AIB}$) increased over time and were fit with a linear regression using linear mixed effects models to give a quantitative measure of the extent of colony polarisation in response to addition of new resources.

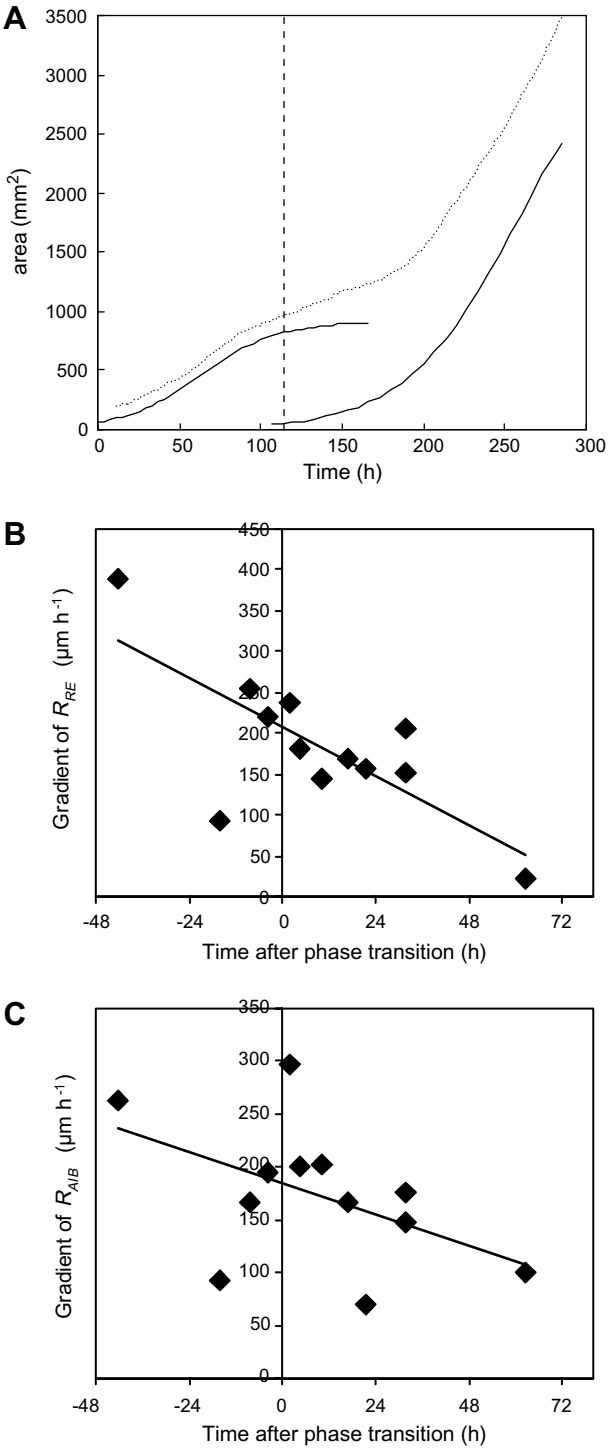

Fig. 4. Attenuation of response sensitivity with developmental age. The total extension, measured as the increase in colony area (A, dotted line), was fit with a bi-logistic equation to separate out two growth phases (solid lines). The first growth phase corresponded to symmetrical extension and the second phase the initiation of asymmetric extension. As the parameters for the first phase were better constrained by the data, the time point corresponding to 90% completion of the first phase (dashed line) was used to define the developmental transition between the two phases. Visually this also corresponded to the start of the 2nd asymmetric extension phase. The decrease in response, measured as the gradient of $\overline{R}_{RE}$ and $\overline{R}_{AIB}$, is shown in B and C, respectively, for the filter paper treatments with respect to the developmental stage of the colony as defined by the time after the end of the first extension phase. The largest response occurred in colonies treated during the symmetrical phase or just as the transition was beginning. More mature colonies that were already committed to asymmetric extension were less responsive.

4. Discussion

4.1. Nutrient limitation triggered a transition to sparser, asymmetrical extension

Initial extension was as a fine, dense reasonably symmetrical colony with uniform allocation of ^{14}C-AIB that is characteristic of colony growth on rich media. After 3–4 days, this growth pattern was replaced by sparser, more asymmetric extension whether or not additional resources were present. As the level of ^{14}C-AIB uptake increased substantially during the transition, we infer that the system was becoming progressively nutrient depleted and suggest that the increase in ^{14}C-AIB uptake occurred as concentrations of utilisable amino acids declined and/or was facilitated by induction of additional amino acid transporters in response to reduced amino acid availability (Wipf et al., 2002). A similar transient phase of dense, even growth also occurs from pre-colonised wood blocks for *P. velutina* in soil microcosms and is reflected in a high initial value of both surface fractal (D_{BS}) and mass fractal (D_{BM}) dimension that decline rapidly with subsequent growth as a more corded network (Boddy et al., 1999).

The mechanism that leads to asymmetric extension from a limited sector of the colony, even in the absence of additional resources, is not known. In several colonies there was clear separation of two extension phases using the bi-logistic analysis, coupled with a distinct change in the morphology of the colony in the second phase. It appears that most of the hyphae in the first phase cease extension and those that continue branch less frequently to give a sparser network. Similar versions of the slow-dense/fast-effuse transition have been reported for several other species (Rayner and Coates, 1987) and are associated with 'point growth' phenomena (Coggins et al., 1980) as the mycelium changes its operational scale (Rayner et al., 1994). In some species, the transition appears to involve a genetic switch that persists in colonies sub-cultured from sectors with different growth behaviour that are then grown in different media (Stenlid and Rayner, 1989). Alternatively there is evidence for the involvement of diffusible factors that may repress growth during the slow-dense phase that can be alleviated by growth on dilute media (Stenlid and Rayner, 1989). Neither of these explanations seems likely to account for the observations for *P. velutina* as the transition between the two extension phases was freely reversible on successive sub-culturing, and it is unlikely that diffusible signals were involved as exploratory extension across the scintillation screen occurred in a dry environment. Thus metabolic control of the morphological switch appears more likely, probably operating through sensing of internal nutrient levels (Watkinson, 1999). Interestingly, the radial extent of the fine mycelium is similar to the maximum predicted from a discontinuous diffusion model of internal nutrient transport through the reticulate vacuole system (Darrah et al., 2006). It is possible that further exploration can only be supported with the introduction of a higher capacity long-distance transport system arising through cord formation.

The early phase of dense growth from an inoculum was distinct from proliferation of fine hyphae in localised patches that occur in corded networks (Wells et al., 1997; Boddy et al., 1999). The latter is thought to represent a transient morphological adaptation to scavenge locally for mineral nutrients in the soil as the probability of patch formation depends on the nutrient balance in the rest of the colony, and increases both if overall mineral nutrient levels are low, and if carbon is high (Wells et al., 1997; Boddy et al., 1999). Likewise, the increase in localised radial extension observed here is distinct from the growth inhibition observed at very high concentrations of AIB when it has fungistatic properties (Watkinson, 1984). There is the possibility that the presence of AIB does have some impact on the responses observed. However, we have previously shown that colonies develop in a similar manner with added cellulose resources in the presence and absence of ^{14}C-AIB (Tlalka et al., 2007).

4.2. Colonies responded as a co-ordinated unit

Addition of a new cellulose resource triggered strong polarisation of the colony with cessation of extension distal from the new resource and tight focus of extension and N-allocation to the sector with the added resource. The new resource provides several stimuli that might have initiated the developmental change, including thigmotropic, osmotic and nutritional cues (Bahn et al., 2007). Whilst some reaction was observed with glass fibre discs that might be expected to mimic touch and osmotic stimuli, the majority of the response appears to be associated with nutritional cues from the cellulose (Table 1). It is also possible that physical contact represents an important early signal, and may even be needed to sensitise the system to detect nutritional cues required for a sustained response. We infer from these results that metabolisable resources triggered a sustained colony-wide response leading to highly focussed extension and resource allocation to the sector of the colony containing the added resource.

The mechanism leading to detection of the cellulose resource is not known. It is likely that the response is not triggered by the cellulose polymers directly, but by freely-diffusible soluble breakdown products. In the case of the pure cellulose discs added here, there are unlikely to be any endogenous soluble sugars present, so the signalling pathway must be initiated following cellulose breakdown by low levels of constitutive extracellular cell wall degrading enzymes (CWDE, Aro et al., 2005). Although it is difficult to ascertain the earliest time-point where there was an unequivocal response, changes in AIB allocation were clearly detectable within 12 h of contact. This would allow plenty of time to sense cellulose by-products of external degradation. Most work on the subsequent internal signal transduction cascades has focussed on further induction of CWDE through conserved transcription factors such as *XlnR, ACEI, ACEII* and the *CCAAT* binding complex (Bahn et al., 2007). Whether the same signal cascades also link to morphological adaptation and long-distance communication or whether these responses are secondary consequences of changing internal metabolite levels from local C-supply or N-depletion through high secretory activity is not known.

In this study, only the addition of a pure cellulose resource in a readily accessible format was examined on the transport of a non-metabolised amino acid analogue as a proxy for N-allocation to a C-rich sink. Natural resources contain varying C:N ratios (Watkinson et al., 2006; Tlalka et al., 2008) which may trigger more complex responses depending on the internal nutrient status of the colony and the overall quality and accessibility of the resource. It would be of interest to determine whether the responses observed here represent a generic reaction to the presence of any new resource, or whether the system is capable of more subtle allocation of internal resources to better match the external nutrient availability.

4.3. Polarised growth occurs at the expense of growth elsewhere in the colony

Whilst it might be expected that additional resources would promote local growth, it is less clear how or why marginal extension elsewhere should cease. Similar changes in growth pattern have been made following addition of wood resources to soil microcosms, in which growth slows or ceases whilst the new resource is colonised (Boddy and Jones, 2007). The magnitude of the response and the delay before new growth emerged from the

resource was dependent both on the size of the resource, and also the size of the initial inoculum. This may represent a simple response to nutrient limitation of growth, or a more sophisticated strategy to colonise and exploit the available resource, particularly in the face of other competing saprotrophs, before risking further exploration. In the data reported here, the cellulose disc was sufficient to trigger polarised extension, but did not significantly delay extension in that sector. There was some evidence that the hyphae directly contacting the resource no longer continued exploration (see Fig. 1C for example), but this sector of the margin was rapidly filled by spread of the hyphae adjacent to the resource. Nevertheless, extension elsewhere in the colony either ceased completely or was reduced substantially following contact with the resource. Interestingly, whilst the average growth rate between different sectors of the colony declined slightly with the onset of polarised extension, the absolute rate in the actively growing regions increased, sometimes quite markedly. Thus, it appears that there is a flexible trade off between the rate of radial expansion and the proportion of the colony margin that is active.

At least part of the variation in the response magnitude was associated with developmental stage after the end of the initial, symmetrical extension phase. It is likely that the fungus would maintain its external resource detection system and ability to exploit the resource whatever the developmental stage, so we infer that the apparent decrease in sensitivity reflects a change in system-wide communication and co-ordination. One possible mechanism for system-wide integration is the result of demand-led competition for resources by the different sectors, with the best-resourced sector winning out. Alternatively, there may be specific mechanisms for long-distance communication using chemical, turgor or electrical signalling (Olsson, 1999, 2001; Cairney, 2005; Read, 2007) that actively shut-down growth in certain sectors and initiate recycling of now redundant material, possibly through apoptotic processes (Olsson, 1999; Thrane et al., 2004).

Co-ordinated, system-wide behaviour has been observed previously for the oscillatory component of ^{14}C-AIB movement that self-organises into domains that differ in the phase of the oscillations (Fricker et al., 2007; Tlalka et al., 2007). Notably, hyphae in the inoculum and added resource had closely related phases, whilst the remainder of the mycelium oscillated nearly 180° out of phase. Interestingly, there is no difference in the oscillatory behaviour of the mycelium in the supplemented sector or in more distal sectors despite the differences in extension rate (Tlalka et al., 2007). Thus oscillations in detectable ^{14}C-AIB do not provide any clues as to the signalling systems that modulate localised extension and N-allocation.

4.4. Does polarised extension represent an adaptive foraging strategy?

Given that the total area covered by the mycelium was essentially the same in control and treated colonies, the potential ecological significance of polarised extension following encounter with a new resource cannot be simply ascribed to greater coverage achieved by the colony. Instead, we infer that the polarisation is a manifestation of an adaptive foraging strategy that increases future return. The prediction would be that localised extension increases the probability of encounter with subsequent resources. In further support of such a view, we note that the AIB response was more marked than the extension response leading to a slight preferential increase in ^{14}C-AIB accumulation over and above that simply expected by the increased localised extension. It is also possible that the local mycelial density increases during polarised growth, leading to a greater biomass and consequent increase in ^{14}C-AIB without any specific preferential accumulation. However, at this stage we do not have non-destructive techniques to simultaneously estimate ^{14}C-AIB distribution and mycelial biomass.

If preferential N-accumulation does occur, it may indicate an element of anticipation, possibly allowing more rapid exploitation of any new resources found during polarised extension. The success of such a strategy is clearly dependent on the spatial pattern of resources in the environment. For example, in either a homogeneous or a random environment all strategies should yield equivalent results. Conversely if resources were placed in a regular lattice, responding to the first encounter would be expected to reduce the probability of encounter with the next resource. The more interesting cases lie in more realistic distributions when resources patterns are likely to show some degree of spatial auto-correlation with varying degrees of clustering. To test whether the polarised extension strategy is adaptive, we are currently developing a foraging model based on parameters derived from the empirical measurements reported here.

Acknowledgments

We gratefully acknowledge financial support from the NERC (GR3/12946 & NER/A/S/2002/882), BBSRC (43/P19284), EU Framework 6 (STREP No. 12999) and from the Dunstan Bequest (University of Oxford). We thank Prof. L. Boddy for detailed comments on the manuscript.

Appendix A. Supplementary data

Supplementary data associated with this article can be found, in the online version, at doi:10.1016/j.fgb.2008.03.015.

References

Aro, N., Pakula, T., Penttila, M., 2005. Transcriptional regulation of plant cell wall degradation by filamentous fungi. FEMS Microbiol. Rev. 29, 719–739.
Bahn, Y.S., Xue, C.Y., Idnurm, A., Rutherford, J.C., Heitman, J., Cardenas, M.E., 2007. Sensing the environment: lessons from fungi. Nat. Rev. Microbiol. 5, 57–69.
Boddy, L., 1999. Saprotrophic cord-forming fungi: meeting the challenge of heterogeneous environments. Mycologia 91, 13–32.
Boddy, L., Donnelly, D.P., 2008. Fractal geometry and microorganisms in the environment. In: Senesi, N., Wilkinson, K. (Eds.), Fractal Structures and Processes in the Environment. IUPAC.
Boddy, L., Jones, T.H., 2007. Mycelial responses in heterogeneous environments: parallels with macroorganisms. In: Fungi in the Environment. Cambridge University Press, pp 112–158.
Boddy, L., Wells, J.M., Culshaw, C., Donnelly, D.P., 1999. Fractal analysis in studies of mycelium in soil. Geoderma 88, 301–328.
Bolton, R.G., Boddy, L., 1993. Characterization of the spatial-aspects of foraging mycelial cord systems using fractal geometry. Mycol. Res. 97, 762–768.
Cairney, J.W.G., 2005. Basidiomycete mycelia in forest soils: dimensions, dynamics and roles in nutrient distribution. Mycol. Res. 109, 7–20.
Coggins, C.R., Hornung, U., Jennings, D.H., Veltkamp, C.J., 1980. The phenomenon of point growth and its relation to flushing and strand formation in mycelium of *Serpula lacrimans*. Trans. Brit. Mycol. Soc. 75, 69–76.
Darrah, P.R., Tlalka, M., Ashford, A., Watkinson, S.C., Fricker, M.D., 2006. The vacuole system is a significant intracellular pathway for longitudinal solute transport in basidiomycete fungi. Eukaryot. Cell 5, 1111–1125.
Donnelly, D.P., Boddy, L., 1998. Developmental and morphological responses of mycelial systems of *Stropharia caerulea* and *Phanerochaete velutina* to soil nutrient enrichment. New Phytol. 138, 519–531.
Donnelly, D.P., Wilkins, M.F., Boddy, L., 1995. An integrated image-analysis approach for determining biomass, radial extent and box-count fractal dimension of macroscopic mycelial systems. Binary 7, 19–28.
Dowson, C.G., Rayner, A.D.M., Boddy, L., 1988a. Foraging patterns of *Phallus impudicus*, *Phanerochaete laevis* and *Steccherinum fimbriatum* between discontinuous resource units in soil. FEMS Microbiol. Ecol. 53, 291–298.
Dowson, C.G., Rayner, A.D.M., Boddy, L., 1988b. Inoculation of mycelial cord-forming Basidiomycetes into woodland soil and litter. 1. Initial establishment. New Phytol. 109, 335–341.
Dowson, C.G., Rayner, A.D.M., Boddy, L., 1988c. Inoculation of mycelial cord-forming Basidiomycetes into woodland soil and litter. 2. Resource capture and persistence. New Phytol. 109, 343–349.
Fricker, M.D., Bebber, D.P., Boddy, L., 2008. Mycelial networks: structure and dynamics. In: Boddy, L., Franklin, J.C., van West, P. (Eds.), Ecology of Saprotrophic Basidiomycetes. Academic Press, Amsterdam.
Fricker, M.D., Tlalka, M., Bebber, D., Takagi, S., Watkinson, S.C., Darrah, P.R., 2007. Fourier-based spatial mapping of oscillatory phenomena in fungi. Fungal Genet. Biol. 44, 1077–1084.

Harris, M.J., Boddy, L., 2005. Nutrient movement and mycelial reorganization in established systems of *Phanerochaete velutina*, following arrival of colonized wood resources. Microb. Ecol. 50, 141–151.

Lindahl, B.J., Ouml, Rn.D., Olsson, S., 2004. Fungal translocation—creating and responding to environmental heterogeneity. Mycologist 18, 79–88.

Olsson, S., 1999. Nutrient translocation and electrical signalling in mycelia. In: Gow, N.A.R., Robson, G.D., Gadd, G.M. (Eds.), The fungal Colony. Cambridge University Press, Cambridge, pp. 25–48.

Olsson, S., 2001. Colonial growth of fungi. In: Howard, R.J., Gow, N.A.R. (Eds.), Biology of the Fungal Cell. Springer, pp. 125–141.

Otsu, N., 1979. Threshold selection method from gray-level histograms. IEEE Trans. Syst. Man Cybernet. 9, 62–66.

Pinheiro, J.C., Bates, D.M., 2000. Mixed-effects Models in S and S-Plus. Springer, New York. 528.

Pizer, S.M., Amburn, E.P., Austin, J.D., Cromartie, R., Geselowitz, A., Greer, T., ter Haar Romeny, B., Zimmerman, J.B., Zuiderveld, K., 1987. Adaptive histogram equalization and its variations. Comput. Vis. Graph. Image Process. 39, 355–368.

R Development Core Team, 2007. A language and environment for statistical computing. R foundation for statistical computing. Vienna, Austria.

Rayner, A.D.M., Coates, D., 1987. Regulation of mycelial organisation and responses. In: Rayner, A.D.M., Braisier, C.M., Moore, D. (Eds.), Evolutionary Biology of the Fungi. Cambridge University Press, Cambridge, pp. 115–136.

Rayner, A.D.M., Griffith, G.S., Ainsworth, A.M., 1994. Mycelial interconnectedness. In: Gow, N.A.R., Gadd, G.M. (Eds.), The Growing Fungus. Chapman and Hall, London, pp. 21–40.

Read, N.D., 2007. Environmental sensing and the filamentous lifestyle. In: Gadd, G.M., Watkinson, S.C., Dyer, P.S. (Eds.), Fungi in the Environment. Cambridge University Press, Cambridge, pp. 38–57.

Stenlid, J., Rayner, A.D.M., 1989. Environmental and endogenous controls of developmental pathways - Variation and its significance in the forest pathogen, *Heterobasidion annosum*. New Phytol. 113, 245–258.

Thrane, C., Kaufmann, U., Stummann, B.M., Olsson, S., 2004. Activation of caspase-like activity and poly (ADP-ribose) polymerase degradation during sporulation in *Aspergillus nidulans*. Fungal Genet. Biol. 41, 361–368.

Tlalka, M., Bebber, D., Darrah, P.R., Watkinson, S.C., Fricker, M.D., 2007. Emergence of self-organised oscillatory domains in fungal mycelia. Fungal Genet. Biol. 44, 1085–1095.

Tlalka, M., Bebber, D.P., Darrah, P.R., Watkinson, S.C., 2008. Mycelial networks: nutrient uptake, translocation and role in ecosystems. In: Boddy, L., Frankland, J.C., West, P.v. (Eds.), Ecology of Saprotrophic Basidiomycetes. Academic Press, Amsterdam, pp. 3–18.

Tlalka, M., Hensman, D., Darrah, P.R., Watkinson, S.C., Fricker, M.D., 2003. Noncircadian oscillations in amino acid transport have complementary profiles in assimilatory and foraging hyphae of *Phanerochaete velutina*. New Phytol. 158, 325–335.

Tlalka, M., Watkinson, S.C., Darrah, P.R., Fricker, M.D., 2002. Continuous imaging of amino-acid translocation in intact mycelia of *Phanerochaete velutina* reveals rapid, pulsatile fluxes. New Phytol. 153, 173–184.

Watkinson, S.C., 1984. Inhibition of growth and development of *Serpula lacrimans* by the non-metabolized amino-acid analog alpha-aminoisobutyric-acid. FEMS Microbiol. Lett. 24, 247–250.

Watkinson, S.C., 1999. Metabolism and hyphal differentiation in large basidiomycete colonies. In: Gow, N.A.R., Gadd, G.M., Robson, G.J. (Eds.), The Fungal Colony. Cambridge University Press, Cambridge, pp. 127–157.

Watkinson, S.C., Bebber, D., Darrah, P.R., Fricker, M.D., Tlalka, M., Boddy, L., 2006. The role of wood decay fungi in the carbon and nitrogen dynamics of the forest floor. In: Gadd, G.M. (Ed.), Fungi in Biogeochemical Cycles. Cambridge University Press, Cambridge, pp. 151–181.

Wells, J.M., Boddy, L., Donnelly, D.P., 1998a. Wood decay and phosphorus translocation by the cord-forming basidiomycete Phanerochaete velutina: the significance of local nutrient supply. New Phytol. 138, 607–617.

Wells, J.M., Donnelly, D.P., Boddy, L., 1997. Patch formation and developmental polarity in mycelial cord systems of *Phanerochaete velutina* on a nutrient-depleted soil. New Phytol. 136, 653–665.

Wells, J.M., Harris, M.J., Boddy, L., 1998b. Encounter with new resources causes polarized growth of the cord-forming basidiomycete *Phanerochaete velutina* on soil. Microb. Ecol. 36, 372–382.

Wipf, D., Ludewig, U., Tegeder, M., Rentsch, D., Koch, W., Frommer, W.B., 2002. Conservation of amino acid transporters in fungi, plants and animals. Trends Biochem. Sci. 27, 139–147.